Parameterization of volume scattering function of coastal waters based on the statistical approach.

A. Sokolov[1,*], M. Chami[2], E. Dmitriev[3], G. Khomenko[1†]

[1] *Laboratoire de PhysicoChimie de l'Atmosphère, Université du Littoral Côte d'Opale & Université Lille Nord de France, 189A Avenue Maurice Schumann 59140, Dunkerque, France*

[2] *Laboratoire d'Océanographie de Villefranche, Universite Pierre et Marie Curie, Quai de la Darse B.P.08, 06238, Villefranche sur Mer, France*

[3] *Institute of Numerical Mathematics of Russian Academy of Science, ul. Gubkina, 8, Moscow, Moscow, 119333, Russia*

** anton.sokolov@univ-littoral.fr*

Abstract: A parameterization of the volume scattering function (VSF) specific to coastal waters is proposed. We have found that the standard VSF parameterizations proposed by Fournier-Forand and Petzold do not fit our measurements obtained with a high angular resolution VSF-meter for water samples taken in the Black Sea coastal zone. We propose modeling VSF as a linear function of scattering, backscattering and particulate absorption. The statistical techniques employed allow us to retrieve the variability of VSF and to demonstrate the significance of the estimates obtained. The results of independent validation and the comparison with other commonly used parameterizations are provided.

OCIS codes: (010.4458) Oceanic scattering; (010.4450) Oceanic optics

References and links

1. C. D. Mobley, Light and Water: Radiative Transfer in Natural Waters, (Academic, San Diego, Calif., 1994)
2. G. Fournier, and J. L. Forand, "Analytic phase function for ocean water," Ocean Optics XII, J. S. Jaffe, ed., Proc. SPIE 2258, 194–201 (1994).
3. A. Morel, and L. Prieur, "Analysis of variations in ocean color," Limnol. Oceanogr. **22**, 709–722 (1977).
4. T. J. Petzold, "Volume Scattering Functions for Selected Ocean Waters," Technical Report SIO 72–78 Scripps Institute of Oceanography, San Diego, Calif. (1972).
5. J.-F. Berthon, E. Shybanov, M. E.-G. Lee, and G. Zibordi, "Measurements and modeling of the volume scattering function in the coastal northern Adriatic Sea," Appl. Opt. **46**(22), 5189–5203 (2007).
6. O. V. Kopelevich, "Small-parameter model of optical properties of sea water," Ocean Opt. **1,** Physical Ocean Optics, ed. A. S. Monin, Nauka (in Russian, 1983).
7. W. Freda, and J. Piskozub, "Improved method of Fournier-Forand marine phase function parameterization," Opt. Express **15**(20), 12763–12768 (2007).
8. M. E. Lee, and M. R. Lewis, "A new method for the measurement of the optical volume scattering function in the upper ocean," J. Atmos. Ocean. Technol. **20**(4), 563–571 (2003).
9. X. Zhang, M. Lewis, M. E.-G. Lee, B. Johnson, and G. K. Korotaev, "The volume scattering function of natural bubble populations," Limnol. Oceanogr. **47**, 1273–1282 (2002).
10. H. Storch, F. W. Zwiers, Statistical Analysis in Climate Research., UK, Cambridge, 484 p. (Cambridge University Press, 2001).
11. S. Wilks, Statistical Methods in the Atmospheric Sciences, Second Edition, International Geophysics Series, **91**, 630 p. (ELSEVIER, 2006).
12. C. D. Rodgers, Inverse methods for atmospheric sounding, theory and practice. World Scientific Series on atmospheric, oceanic and planetary physics, **2**. Singapore, p. 240. (World Scientific, 2000).
13. R. Daley, Atmospheric Data Analysis, Cambridge atmospheric and space science series. p. 458 (Cambridge U. Press, 1999).
14. C. Davison, and V. D. Hinkley, Bootstrap Methods and Their Application (Cambridge U. Press, 1997).

#120150 - $15.00 USD Received 30 Nov 2009; revised 6 Jan 2010; accepted 12 Jan 2010; published 22 Feb 2010

15. A. Eliassen, Provisional report on calculation of spatial covariance and autocorrelation of the pressure field. Dynamic Meterology: Data Assimilation Methods, L. Bengtsson, M. Ghil, and E. Källen, Eds., Springer-Verlag, 319–330. (1954)
16. A. Sokolov, Modeling of satellite experiment of vertical atmospheric temperature and humidity profiles retrieval by measurements in IR region of spectra, Moscow, Russia, 117p. (PhD thesis in Russian, 2005)
17. M. Chami, E. B. Shybanov, T. Y. Churilova, G. A. Khomenko, M. E.-G. Lee, O. V. Martynov, G. A. Berseneva, and G. K. Korotaev, "Optical properties of the particles in the Crimea coastal waters (Black Sea)," J. Geophys. Res. **110**(C11), C11020 (2005).
18. M. Chami, E. B. Shybanov, G. A. Khomenko, M. E.-G. Lee, O. V. Martynov, and G. K. Korotaev, "Spectral variation of the volume scattering function measured over the full range of scattering angles in a coastal environment," Appl. Opt. **45**(15), 3605–3619 (2006).
19. E. V. Dmitriev, G. Khomenko, M. Chami, A. A. Sokolov, T. Y. Churilova, and G. K. Korotaev, "Parameterization of light absorption by components of seawater in optically complex coastal waters of the Crimea Peninsula (Black Sea)," Appl. Opt. **48**(7), 1249–1261 (2009).
20. C. D. Mobley, L. K. Sundman, and E. Boss, "Phase function effects on oceanic light fields," Appl. Opt. **41**(6), 1035–1050 (2002).
21. J. H. Mathews, and K. D. Fink, Numerical Methods Using MATLAB, Third Edition, (Prentice Hall, 1999).
22. G. Mitchell, and D. A. Kiefer, "Chlorophyll a specific absorption and fluorescence excitation spectra for light limited phytoplankton," Deep-Sea Res. **35**(5), 639–663 (1988).
23. M. Kishino, N. Takahashi, N. Okami, and S. Ichimura, "Estimation of the spectral absorption coefficients of phytoplankton in the sea," Bull. Mar. Sci. **37**, 634–642 (1985).
24. C. S. Yentsch, "Measurement of visible light absorption by particulate matter in the ocean," Limnol. Oceanogr. **7**, 207–217 (1962).
25. C. D. Mobley, and L. K. Sundman, HYDROLIGHT 4.1 Technical Documentation (Sequoia Scientific, Inc., Redmond, Wash., 2000).
26. H. Loisel, and A. Morel, "Light scattering and chlorophyll concentration in case I waters," Limnol. Oceanogr. **43**, 847–858 (1998).

1. Introduction

The remote sensing of sea coastal waters is widely used in different applications of ecological monitoring, climate modeling, fishing and many others for the retrieval of parameters characterizing the content of particulate and dissolved substances. The spectral remote sensing reflectance (Rrs) measured by satellite instruments is used as an input parameter in solving the related forward and inverse problems of radiative transfer for the system "sea water – atmosphere". The volume scattering function (VSF) is one of the basic inherent optical properties (IOP) [1] influencing the flux of radiation upwelling from the water surface. Presently the most advanced algorithms for the processing and the interpretation of satellite imagery employ VSF to solve radiative transfer equation. On the other hand, the measurements reveal the high variability of VSF for different types of sea water, especially in coastal areas. Thus, the case specific VSF modeling is needed.

A theoretical model proposed by Fournier-Forand (FF) [2] can be used for VSF simulation. This technique is based on an analytical expression for the phase function of spherical Mie scatterers with a hyperbolic (Junge-type) particle size distribution. The FF phase function is expressed by two parameters, real index of refraction n and slope of the Junge particle size distribution μ. These assumptions do not perfectly correspond to the real waters with suspended complex particles. In coastal waters (case 2 waters according to Morel [3]) with a high content of suspended inorganic matter, the theoretical VSF simulations are not exact enough and the standard remote sensing algorithms fail.

At present there are only a few VSF parameterisations based on real measurements. One of the commonly used was proposed by Petzold [4]. The parameterisation is based on data collected more than 30 years ago and comprises three VSF model curves for different water types. The first was obtained for the turbid water of San Diego Harbor, California; the second comes from near-shore coastal water in San Pedro Channel, California. The third presents very clear water in the Tongue of the Ocean, Bahama Islands. The employed measurements were taken at one wavelength and have a relatively poor angular and spectral resolution.

Another recent parameterisation presented at [5] is based on Kopelevich model [1, 6], and measurements obtained by VSF-meter in the coastal northern Adriatic Sea. This model

#120150 - $15.00 USD Received 30 Nov 2009; revised 6 Jan 2010; accepted 12 Jan 2010; published 22 Feb 2010

separates the contributions by "small" and "large" particles to the particulate scattering. Small particles are taken to be mineral particles less than 1 μm in size with an index of refraction (relative to water) of n = 1.15; large particles are biological particles larger than 1 μm in size with an index of refraction of n = 1.03. The Kopelevich model parameters are estimated as linear functions of the total scattering [5]. A new method of VSF modeling including backscattering, scattering and the absorption data is presented in a recent paper [7]. This technique is based on fitting FF theoretical functions to the measurement data. We will discuss the applicability of this approach to our data in section 4. Unlike the work [7] we propose the statistical modeling of VSF as a function of the scattering, backscattering and spectral absorption.

The construction and validation of the proposed parameterization are based on our data obtained during the field measurement campaigns carried out in 2002, 2003 and 2004 on the oceanographic platform located in the Black Sea. More than 1000 coastal water samples from different depths were collected with a VSF-meter developed by Marine Hydrophysical Institute (Ukraine) [8, 9] The VSF was measured over a large range of angles and at high angular resolution for different wavelengths. We use multivariate statistical estimation techniques to simulate VSF as a function of scattering, backscattering and spectral absorption coefficient.

This paper is organised as follows: in section 2 we start with the definition of the VSF, phase function, scattering and backscattering and introduce the basic statistical methods used in our model. The description of our measurements and results of the statistical analysis of the data are presented in section 3. In section 4 we derive our VSF parameterization on the basis of the data collected in 2002 and then we perform the analysis of our parameterization in section 5. Finally, in section 6, we discuss the results of validation on the data of 2002-2004 and compare it with FF parameterization and Petzold data.

2. Theoretical backgrounds

2.1 Light transmission in medium

The light propagation in water is defined by the spectral absorption coefficient and volume scattering function [1]. Consider a small volume ΔV, of thickness Δr, illuminated by a narrow collimated monochromatic light beam.

The spectral absorption $a\left[m^{-1}\right]$ is defined as ratio of incident $\Phi_i(\lambda)$ and absorbed energy $\Phi_a(\lambda)$ divided by thickness of the absorbing layer:

$$a(\lambda) = \lim_{\Delta r \to 0} \frac{\Phi_a(\lambda)/\Phi_i(\lambda)}{\Delta r}. \tag{1}$$

Similarly, the volume scattering function $\beta\left[m^{-1}sr^{-1}\right]$ is the portion of energy scattered at the angle θ with respect to the transmitted light direction:

$$\beta(\theta,\lambda) = \lim_{\Delta r \to 0} \lim_{\Delta\Omega \to 0} \frac{\Phi_s(\theta,\lambda)/\Phi_i(\lambda)}{\Delta r \Delta\Omega}. \tag{2}$$

The integral of VSF with θ over the whole unit sphere or backward hemisphere gives respectively spectral scattering b and backscattering b_b coefficients:

$$b(\lambda) = 2\pi \int_0^{\pi} \beta(\theta,\lambda)\sin(\theta)\,d\theta, \tag{3}$$

$$b_b(\lambda) = 2\pi \int_{\pi/2}^{\pi} \beta(\theta,\lambda)\sin(\theta)\,d\theta. \tag{4}$$

#120150 - $15.00 USD Received 30 Nov 2009; revised 6 Jan 2010; accepted 12 Jan 2010; published 22 Feb 2010

The spectral volume scattering phase function $\tilde{\beta}(\theta,\lambda)$ is defined by

$$\tilde{\beta}(\theta,\lambda)=\frac{\beta(\theta,\lambda)}{b(\lambda)}. \tag{5}$$

2.2 Statistical linear estimations and bootstrapping technique

In our model the VSF, scattering, backscattering and (optionally) absorption coefficient data are considered as linearly dependent random variables. We employed statistical techniques such as optimal linear estimation [10–13] and the bootstrapping [14] to fit the unknown parameters and verify the results. In general case, the model can be written as

$$\hat{\boldsymbol{\beta}}-\boldsymbol{\beta}^0=\hat{\mathbf{R}}\cdot\left(\mathbf{b}-\mathbf{b}^0\right), \tag{6}$$

where $\hat{\mathbf{R}}$ is an estimate of multiple linear regression matrix ("^" denotes an estimate), $\hat{\boldsymbol{\beta}}$ is a vector of the dimension M with VSF values at different angles, $\mathbf{b}$ is the vector with elements representing the measured values of scattering, backscattering and absorption coefficient, $\boldsymbol{\beta}^0=E(\boldsymbol{\beta})$, $\mathbf{b}^0=E(\mathbf{b})$, E denotes an expectation.

In the simple multiple linear regression method the optimal matrix $\mathbf{R}$ is found analytically by the minimization of the residual variances [10, 11, 13]. It can be written as follows:

$$\mathbf{R}=\mathbf{S}_{\beta b}\mathbf{S}_{\mathbf{b}}^{-1}, \tag{7}$$

where the covariance $\mathbf{S}_{\beta b}=E\left(\left(\boldsymbol{\beta}-\boldsymbol{\beta}^0\right)\left(\mathbf{b}-\mathbf{b}^0\right)^T\right)$ and $\mathbf{S}_{\mathbf{b}}=E\left(\left(\mathbf{b}-\mathbf{b}^0\right)\left(\mathbf{b}-\mathbf{b}^0\right)^T\right)$. In practice, exact covariance matrices are unknown. Thus, some optimal estimates obtained from statistical data are used instead of the exact one and in this case we consider the estimate $\hat{\mathbf{R}}$ of the matrix $\mathbf{R}$. We suppose here and below, that square covariance matrixes are nondegenerate and well-conditioned. The important property of the multivariate regression is that the estimate $\hat{\boldsymbol{\beta}}$ belongs to the same linear subspace that the exact vector $\boldsymbol{\beta}$.

In the case when the linear dependence of $\mathbf{b}$ on $\boldsymbol{\beta}$ exists, that is:

$$\mathbf{b}=\mathbf{A}\boldsymbol{\beta}, \tag{8}$$

$\mathbf{A}$ is a matrix, Eq. (7) can be transformed taking into account that $\mathbf{S}_{\beta b}=\mathbf{S}_{\beta}\mathbf{A}^{\mathbf{T}}$, $\mathbf{S}_{\beta}=E\left(\left(\boldsymbol{\beta}-\boldsymbol{\beta}^0\right)\left(\boldsymbol{\beta}-\boldsymbol{\beta}^0\right)^T\right)$ to the following expression:

$$\mathbf{R}_{\mathbf{b}}^{\mathbf{A}}=\mathbf{S}_{\beta}\mathbf{A}^T\left(\mathbf{A}\mathbf{S}_{\beta}\mathbf{A}^T\right)^{-1}=\mathbf{S}_{\beta}\mathbf{A}^T\mathbf{S}_{\mathbf{b}}{}^{-1}. \tag{9}$$

This estimation coincides with maximum likelihood solution [12] or optimal interpolation estimate [12, 15, 16] when Eq. (8) is exact. In this case the matrix $\hat{\mathbf{R}}_{\mathbf{b}}^{\mathbf{A}}$ satisfies:

$$\mathbf{A}\mathbf{R}_{\mathbf{b}}^{\mathbf{A}}=\mathbf{I}, \tag{10}$$

where I is a unit matrix, and

$$\mathbf{A}\hat{\boldsymbol{\beta}}=\mathbf{b}. \tag{11}$$

If variables are not consistent with a normal distribution, one cannot successfully apply the standard methods for constructing confidence intervals that are commonly based on

#120150 - $15.00 USD Received 30 Nov 2009; revised 6 Jan 2010; accepted 12 Jan 2010; published 22 Feb 2010

Student's distribution or *F* distribution (see [11] for a complete description of the standard statistical methods). Therefore the so-called "bootstrap method" [14] was used to estimate the confidence intervals for the stochastic quantities.

Parametric techniques calculate a distribution function of the estimated parameter from the distribution function of the population, which is supposed to be known. In contrast, the bootstrap method allows us to estimate confidence intervals without this latter hypothesis. The bootstrap method is based on the generation of several sets of samples (so-called bootstrap samples) using the original measurements. Each bootstrap sample is created using a random sampling of the measured data. Every sample is returned to the original data set after selection. Therefore, when constructing a bootstrap sample, a particular data point from the original data set could appear multiple times. Using the various generated bootstrap samples, the procedure allows us to resample the measurement data as many times as we need for the construction of an empirical cumulative distribution function that enables us to establish the uncertainty of the statistical estimates.

3. Materials, measurements and data processing

In situ measurements of the VSF were carried out during field experiments conducted in the Black Sea coastal area in summers 2002, 2003 and 2004. In total more than 1000 VSF profiles were obtained for a variety of meteorological conditions. Here we give a brief description of the experiment and refer to [17–19] for more details. The data were collected from an oceanographic platform located 600 m off the southern coast of the Crimean peninsula. Seawater samples were collected at depths of 0, 4, 8, 12, 16, and 20 m at 11:00 and 14:00, local time. The VSF was measured using the VSF-meter (VSM) [8, 9], (developed by the Marine Hydrophysical Institute, Ukraine, in cooperation with Satlantic Inc. Canada). The VSM allows measurements of the VSF $\beta_\nu(\theta)$ from 0.7° to 178° with an angular resolution of about 0.3°. The VSM is equipped with a revolving wheel of three colour filters with centre wavelengths at 443 nm, 490 nm, 555 nm and 620 nm and therefore it allows us to measure VSF in 4 spectral channels with the bandwidth of 10 nm.

Since one of the objective of the VSF parameterization proposed in the current study is to account for the dependence between the absorption and scattering processes in the water the absorption coefficients values which is collocated with VSF measurements are required. Therefore, only VSF data for which absorption values were available were analyzed for this study. Such a restriction significantly reduces the number of selected VSF measurements. Typically 40% of VSF measurements were rejected due to this constraint.

Then, once the selection of VSF data together with available absorption data was performed, a filtration procedure was applied to VSF measurements to remove data that were affected by unrealistic peaks or noise. These data are meaningless from a physical point of view. They needed to be removed from the data set so that only reliable VSF measurements having a physical meaning were used for the study. Two criteria were used to filter the VSF data. Only samples that satisfied the two following inequalities were selected:

$$\beta(\theta \geq 0.6°) \leq p, \quad \frac{1}{\beta}\frac{d^2\beta}{d\theta^2} \leq q, \tag{12}$$

where $p = 200\left[\mathrm{m^{-1}sr^{-1}}\right]$ and $q = 5\left[\mathrm{deg^{-2}}\right]$. Note that the values of p and q were derived after several tests. The first inequality in Eq. (12) is used to remove the unrealistic peaks of the VSF at small scattering angles. In other words, it allows restricting the maximum VSF value at small angles within a realistic physical range. The second criterion (i.e., the second inequality in equation Eq. (12)) deals with the smoothness of the VSF. The VSF data showing significant noise at some angle were filtered and removed. as an example, the application of Eq. (12) led to the removal of 40 VSF data out of 444 measurements for the data set collected

#120150 - $15.00 USD Received 30 Nov 2009; revised 6 Jan 2010; accepted 12 Jan 2010; published 22 Feb 2010

in 2002. Note that the low rate of rejection also illustrates the good quality of the data provided by the VSM instrument (i.e., low noise in the instrument).

We checked if the measured VSF values are consistent with a normal distribution using Lilliefors and Jarque-Bera tests [11]. The hypothesis that the distribution is normal was rejected at 5% significance level at nearly all angular range for each wavelength (see Fig. 1). Thus the commonly used tests based on the assumption of normality of the population distribution are inapplicable. Thus, the use of bootstrapping technique [14] rather than parametric tests for the confidence intervals estimation is justified.

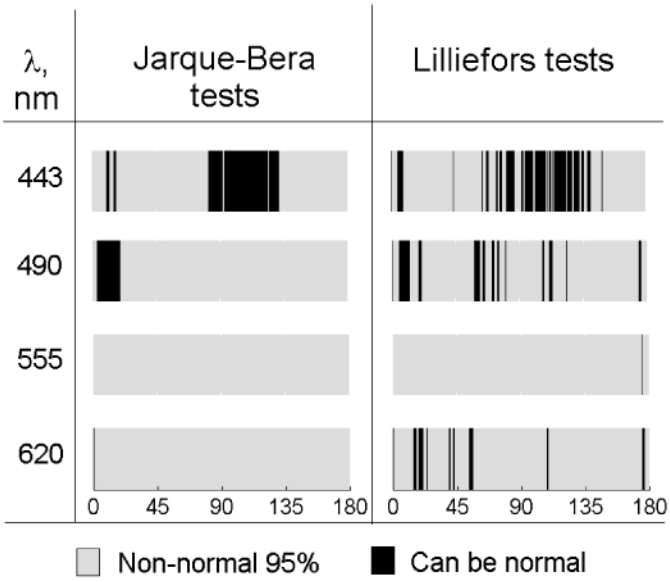

Fig. 1. Tests of normal distribution for the components of VSF. The second column represents the results of the test of Jarque–Bera, the third represents the Lilliefors test for the full angular range at different wavelengths. The significance level is 0.05.

The mean VSF values calculated from data of 2002 at four wavelengths are presented in Fig. 2. The doubled standard deviation interval at 555 is also depicted in the figure by the dotted line. These data are also tabulated in the Table 1. The last two columns (in boldface) present the mean value and the standard deviation averaged over the wavelengths. The values of VSF at angles less than 0.6 and more than 178 degrees were obtained by the extrapolation. They are italicized in the Table 1.

#120150 - $15.00 USD Received 30 Nov 2009; revised 6 Jan 2010; accepted 12 Jan 2010; published 22 Feb 2010

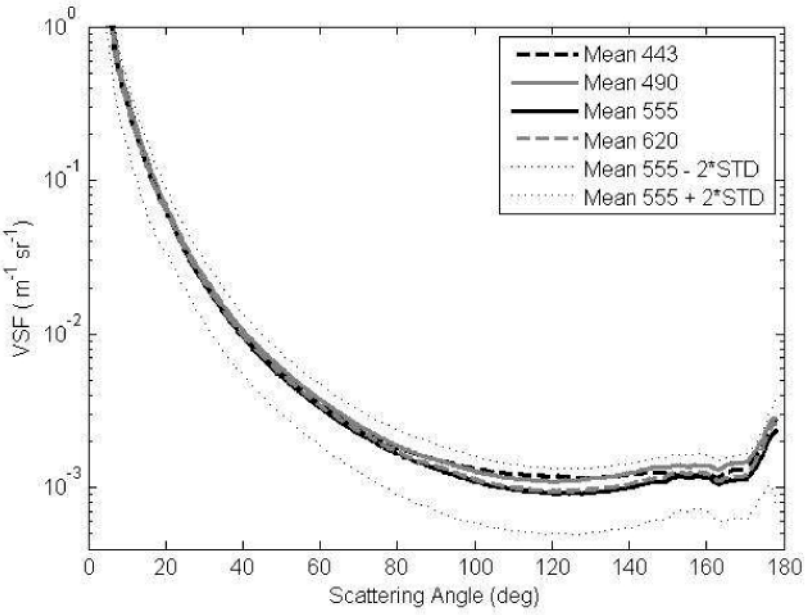

Fig. 2. Averaged VSF at 443, 490, 555 and 620 nm and the doubled standard deviation at 555 nm as a function of scattering angle, based on field experiment data at coastal area of Black Sea in July – August 2002.

To test the reliability of the statistical estimates, we calculated the confidence intervals by using the bootstrapping technique. It appears that the width of the confidence interval for the average VSF is about 10% of mean VSF value, and 35% for the standard deviation at the 5% significance level.

The VSF was interpolated to the grid to provide an angular resolution of 0.1° and extrapolated up to the angular values 0.01° and 180°. It should be mentioned that scattering values and, therefore, the parameterization strongly depend on the type of interpolation and extrapolation at extreme angles. We apply the approach of Mobley et al [20] for VSF extrapolation and spline technique for interpolation [21].

To characterise our data set, we compared our mean phase function with FF theoretical functions and Petzold measurements (Fig. 3 and Fig. 4). The central thick curve corresponds to our measurements of 2002 with bandwidth of 10 nm and the dashed lines depict doubled standard deviation.

As we can see in Fig. 3, the shapes of all the VSF are in general similar; nevertheless some details can be noticed at high angles. The increase of VSF at high angles (more than 170°) is greater than was estimated from Fournier-Forand functions or by extrapolations of Petzold measurements. One can also notice a small hump at 155 degrees.

#120150 - $15.00 USD Received 30 Nov 2009; revised 6 Jan 2010; accepted 12 Jan 2010; published 22 Feb 2010

Table 1. The mean VSF β_0 [$m^{-1}sr^{-1}$] and the standard deviation $\sigma(\beta)$ as a function of angle: at fixed wavelengths (columns 2-9) and the values of these parameters averaged over the wavelengths (last two bold columns), based on 2002 data*.

λ, *nm*	443		490		555		620		**Averaged**	
θ, °	Mean	Std	Mean	Std	Mean	Std	Mean	Std	**Mean**	**Std**
0.01	*7.45E3*	*3.25E4*	*6.52E3*	*1.40E4*	*7.27E3*	*1.51E4*	*1.08E4*	*1.94E4*	***8.01E3***	***2.15E4***
0.1	*417.86*	*462.43*	*449.36*	*318.79*	*451.14*	*330.02*	*585.71*	*412.74*	***476.02***	***389.58***
0.3	*127.33*	*62.27*	*136.18*	*53.83*	*130.97*	*55.30*	*157.97*	*67.84*	***138.11***	***61.02***
0.6	62.37	19.72	65.57	18.80	61.53	19.52	70.83	23.06	**65.08**	**20.59**
1	36.39	9.00	37.64	8.44	34.80	9.02	38.56	9.93	**36.85**	**9.19**
1.5	22.83	6.31	23.24	5.96	21.31	6.30	23.20	6.64	**22.65**	**6.33**
2	14.20	3.93	14.26	3.63	13.05	3.85	14.03	3.87	**13.88**	**3.84**
3	6.22	1.63	6.13	1.46	5.50	1.53	5.84	1.49	**5.92**	**1.55**
5	1.84	0.46	1.79	0.40	1.55	0.41	1.58	0.40	**1.69**	**0.44**
10	3.42E-1	8.46E-2	3.38E-1	7.60E-2	2.98E-1	7.55E-2	2.96E-1	7.28E-2	**3.18E-1**	**8.01E-2**
15	1.33E-1	3.37E-2	1.34E-1	3.26E-2	1.19E-1	3.40E-2	1.17E-1	3.16E-2	**1.26E-1**	**3.39E-2**
20	6.46E-2	1.57E-2	6.54E-2	1.51E-2	5.96E-2	1.64E-2	5.94E-2	1.51E-2	**6.23E-2**	**1.58E-2**
25	3.57E-2	8.34E-3	3.65E-2	8.00E-3	3.31E-2	9.01E-3	3.39E-2	7.84E-3	**3.48E-2**	**8.39E-3**
30	2.23E-2	5.33E-3	2.25E-2	5.20E-3	2.04E-2	5.54E-3	2.11E-2	5.03E-3	**2.16E-2**	**5.33E-3**
40	1.01E-2	2.33E-3	1.02E-2	2.34E-3	9.21E-3	2.51E-3	9.51E-3	2.38E-3	**9.75E-3**	**2.42E-3**
50	5.59E-3	1.30E-3	5.78E-3	1.29E-3	5.12E-3	1.43E-3	5.30E-3	1.33E-3	**5.45E-3**	**1.36E-3**
60	3.43E-3	7.95E-4	3.64E-3	8.50E-4	3.21E-3	8.83E-4	3.32E-3	8.60E-4	**3.40E-3**	**8.60E-4**
70	2.33E-3	5.39E-4	2.47E-3	5.94E-4	2.18E-3	6.14E-4	2.25E-3	6.02E-4	**2.31E-3**	**5.96E-4**
80	1.78E-3	3.84E-4	1.82E-3	4.44E-4	1.60E-3	4.62E-4	1.65E-3	4.61E-4	**1.71E-3**	**4.46E-4**
90	1.49E-3	3.13E-4	1.47E-3	3.41E-4	1.28E-3	3.71E-4	1.33E-3	3.74E-4	**1.39E-3**	**3.61E-4**
100	1.30E-3	2.66E-4	1.25E-3	2.91E-4	1.06E-3	3.14E-4	1.10E-3	3.09E-4	**1.18E-3**	**3.11E-4**
110	1.22E-3	2.42E-4	1.12E-3	2.62E-4	9.47E-4	2.82E-4	9.74E-4	2.63E-4	**1.07E-3**	**2.84E-4**
120	1.16E-3	2.40E-4	1.08E-3	2.52E-4	8.93E-4	2.66E-4	9.28E-4	2.46E-4	**1.02E-3**	**2.73E-4**
130	1.15E-3	2.37E-4	1.12E-3	2.66E-4	9.04E-4	2.69E-4	9.49E-4	2.50E-4	**1.03E-3**	**2.76E-4**
140	1.19E-3	2.47E-4	1.22E-3	2.85E-4	9.72E-4	2.85E-4	1.03E-3	2.52E-4	**1.10E-3**	**2.87E-4**
150	1.22E-3	2.59E-4	1.33E-3	2.95E-4	1.08E-3	2.99E-4	1.16E-3	2.69E-4	**1.20E-3**	**2.95E-4**
155	1.14E-3	2.32E-4	1.33E-3	2.59E-4	1.13E-3	2.85E-4	1.20E-3	2.54E-4	**1.20E-3**	**2.70E-4**
160	1.16E-3	2.53E-4	1.35E-3	2.70E-4	1.13E-3	2.89E-4	1.20E-3	2.56E-4	**1.21E-3**	**2.80E-4**
165	1.22E-3	2.85E-4	1.35E-3	3.00E-4	1.06E-3	3.01E-4	1.12E-3	2.74E-4	**1.19E-3**	**3.09E-4**
170	1.29E-3	3.18E-4	1.43E-3	3.25E-4	1.11E-3	3.27E-4	1.17E-3	2.85E-4	**1.25E-3**	**3.36E-4**
172	1.45E-3	3.56E-4	1.61E-3	3.55E-4	1.25E-3	3.57E-4	1.35E-3	3.08E-4	**1.41E-3**	**3.68E-4**
174	1.75E-3	4.11E-4	1.92E-3	4.20E-4	1.50E-3	4.12E-4	1.67E-3	3.65E-4	**1.71E-3**	**4.30E-4**
175	1.97E-3	4.72E-4	2.14E-3	4.84E-4	1.68E-3	4.67E-4	1.90E-3	4.30E-4	**1.92E-3**	**4.91E-4**
176.1	2.30E-3	5.75E-4	2.49E-3	6.15E-4	1.96E-3	5.65E-4	2.25E-3	5.63E-4	**2.25E-3**	**6.07E-4**
177	2.54E-3	6.90E-4	2.70E-3	7.68E-4	2.16E-3	6.69E-4	2.49E-3	7.18E-4	**2.47E-3**	**7.37E-4**
177.3	2.60E-3	7.44E-4	2.74E-3	8.29E-4	2.20E-3	7.13E-4	2.52E-3	7.75E-4	**2.52E-3**	**7.88E-4**
177.6	2.66E-3	8.12E-4	2.75E-3	8.95E-4	2.24E-3	7.67E-4	2.53E-3	8.34E-4	**2.55E-3**	**8.47E-4**
178	2.73E-3	9.35E-4	2.76E-3	9.91E-4	2.29E-3	8.58E-4	2.53E-3	9.23E-4	**2.58E-3**	**9.43E-4**
179	*2.73E-3*	*9.39E-4*	*2.76E-3*	*9.92E-4*	*2.29E-3*	*8.59E-4*	*2.53E-3*	*9.25E-4*	***2.58E-3***	***9.45E-4***
180	*2.73E-3*	*9.39E-4*	*2.76E-3*	*9.92E-4*	*2.29E-3*	*8.59E-4*	*2.53E-3*	*9.25E-4*	***2.58E-3***	***9.45E-4***

*The extrapolated values are in italics. Two last bold columns contain the values averaged over all wavelengths. The data are provided with a low angular resolution. The high resolution data can be obtained on request to the authors.

#120150 - $15.00 USD Received 30 Nov 2009; revised 6 Jan 2010; accepted 12 Jan 2010; published 22 Feb 2010

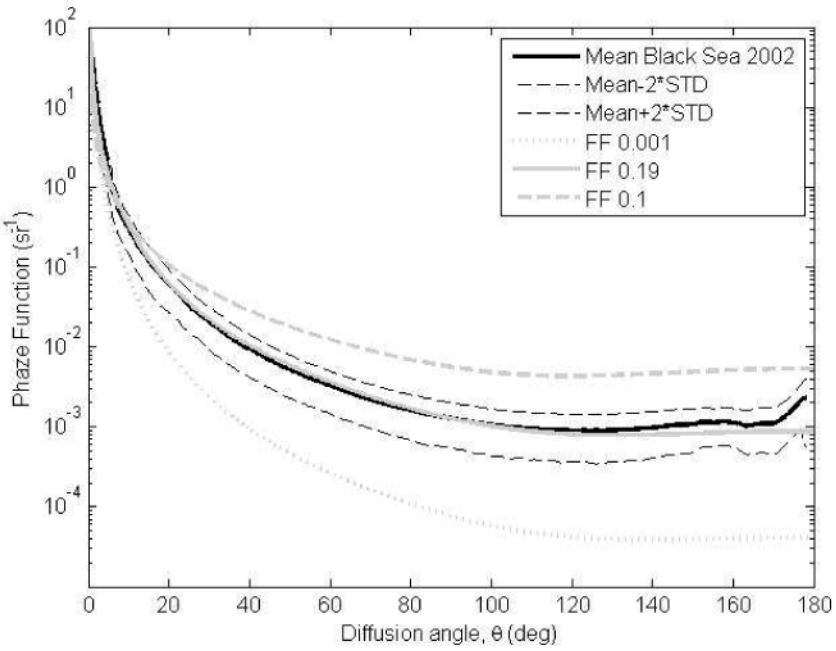

Fig. 3. Comparisons of Black Sea 2002 mean phase function with Fournier-Forand analytical phase functions. Scattering to backscattering ratio for our VSF (the black curve) is about 0.019.

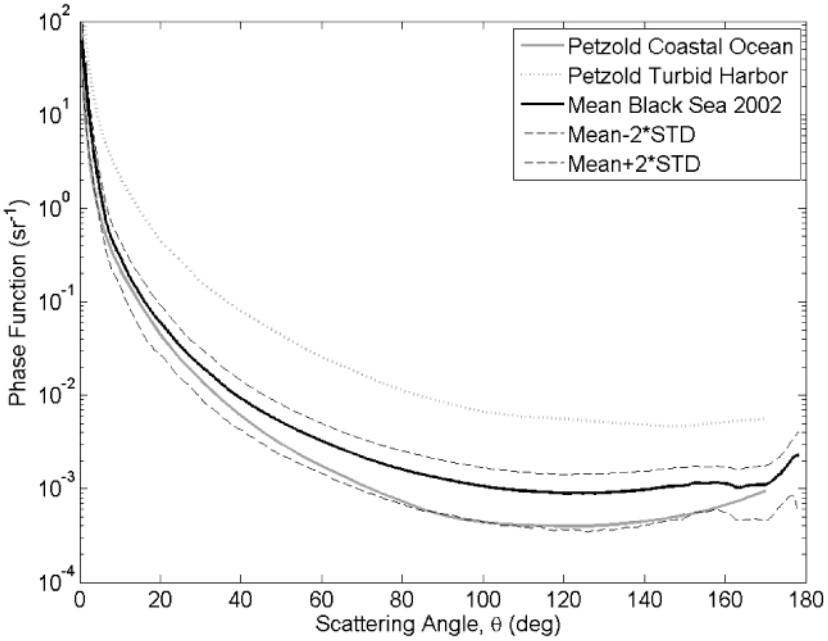

Fig. 4. Comparisons of Black Sea 2002 mean phase function with phase functions derived from Petzold measurements.

It has been shown in a previous paper [18] based on calibration experiments using spherical beads that the uncertainties of the instrument that was used to acquire the VSF measurements employed in the current study are within 5%. These experiments showed that

#120150 - $15.00 USD Received 30 Nov 2009; revised 6 Jan 2010; accepted 12 Jan 2010; published 22 Feb 2010

there is no significant biases between Mie theory and VSF measurements in the angular range 170-180° and at 155°.

A similar version of the VSM instrument was used in 2004 in the coastal northern Adriatic Sea [5]. As in the Black Sea campaign, Berthon et al.'s calibration experiment [5] did not show any specific features of the VSF in the angular range 170-180 deg. Therefore, based on these calibration experiments, one could think that the increase of the VSF in the range 170-180° observed in the data presented in the current study should not be due to significant uncertainties of the VSM instrument but more likely to some effects of particles scattering.

The VSF shape observed around a scattering angle of 155° is probably due to the optical properties of the particles encountered in the Black Sea waters. Indeed, since such a behaviour was not observed during the Black Sea calibration beads experiments [18] and in other waters like Adriatic Sea as well [5]. It is likely that the hump at 155° is not due to an artefact of the VSM instrument. The hump of VSF observed at this scattering angle could be due to high proportion of suspended mineral-like particles with high refractive index in coastal waters. Mie calculations of VSF for waters showing a prevailing composition of highly refractive particles (i.e., refractive index greater than 1.2) were performed and confirmed that such type of particles can lead to the occurrence of a hump around the scattering angle of 155°.

The influence of the hump observed in the VSF around 155° on the backscattering values Eq. (4) is weak (our calculations showed that it is less than 2%) because of the occurrence of the sinus function in Eq. (4).

The integration of β over whole unit sphere and the backward hemisphere provides the scattering b and backscattering b_b coefficients. The mean values and the standard deviations of b and b_b are presented in Table 2 for each wavelength and for the averaged by wavelength values (in boldface). In some applications it is common to employ a phase function instead of VSF. The mean phase functions $\tilde{\beta}^0$ can be easily obtained from Eq. (5) by using the data in Table 1 and Table 2.

Table 2. The average values and standard deviations of scattering b_λ^0 [m^{-1}] and backscattering $b_{b\lambda}^0$ [m^{-1}] at various wavelength calculated by the VSFs measured in 2002*.

λ, *nm*	443		490		555		620		**Averaged**	
	Mean	Std	Mean	Std	Mean	Std	Mean	Std	**Mean**	**Std**
b_λ^0, m^{-1}	0.38	0.11	0.38	8.9E-2	0.34	9.2E-2	0.37	9.9E-2	**0.366**	**9.8E-2**
$b_{b\lambda}^0, m^{-1}$	7.7E-3	1.6E-3	7.6E-3	1.8E-3	6.4E-3	1.8E-3	6.7E-3	1.8E-3	**7.12E-3**	**1.84E-3**

*Two last bold columns contain the values averaged over all wavelengths.

Our measurements exhibit significant variability with respect to the average value. The ratio of the standard deviation of the VSF and mean value of the VSF is nearly constant (see Fig. 5) for non-interpolated VSF values:

$$\Delta(\theta) = \frac{\sigma(\beta(\theta))}{E(\beta(\theta))} \approx 0.26. \quad (13)$$

#120150 - $15.00 USD Received 30 Nov 2009; revised 6 Jan 2010; accepted 12 Jan 2010; published 22 Feb 2010

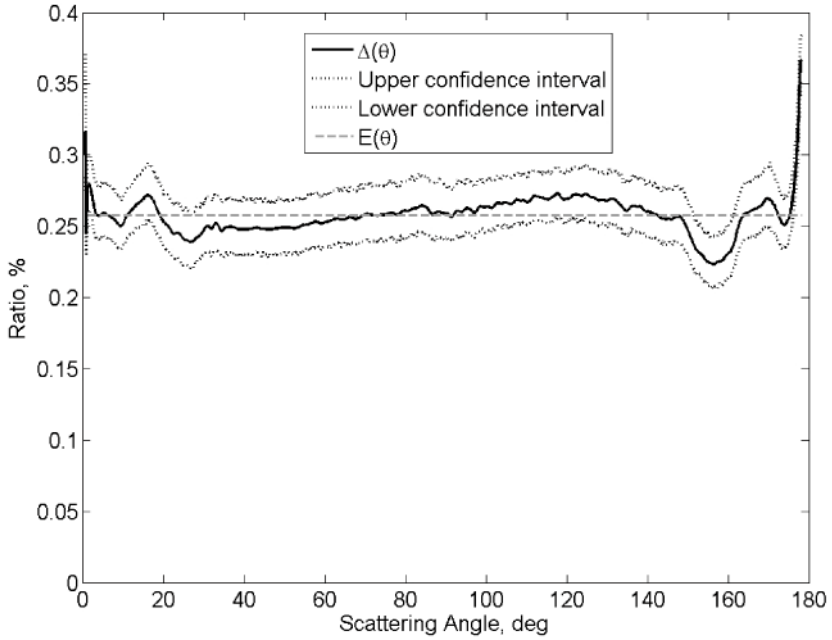

Fig. 5. The estimation of the ratio of standard deviation of VSF to mean VSF Δ(θ) and 95% confidence interval. The value averaged over the angles presented by the dashed line.

To account for this variability, we have created a VSF model based on scattering, backscattering and (optionally) on absorption data. The spectral particulate absorption was measured simultaneously with VSF values using the methods described in [22–24]. The description and statistical characteristics of our absorption data set can be found in [17, 19]. In our model we considered the absorption at 412, 440, 488, 510, 532, 555, 650, 676 and 715 nm, which corresponds to channels of Wetlabs AC-9 instrument (Wetlabs Inc.). The mean values and the standard deviations of absorption calculated by the 2002 data are presented in Table 3.

Table 3. The average values and standard deviations of absorption measured in 2002. The wavelengths correspond to channels of Wetlabs AC-9 instrument.

λ , *nm*	412	440	488	510	532	555	650	676	715
a_λ^0, m^{-1}	11.7E-2	10.8E-2	7.3E-2	5.4E-2	3.9E-2	2.7E-2	1.1E-2	2.2E-2	1.6E-3
$\sigma(a_\lambda^0), m^{-1}$	3.7E-2	3.1E-2	1.8E-2	1.4E-2	1.1E-2	8.8E-3	3.6E-3	7.8E-3	5.2E-4

4. Development of the VSF model

We propose here a model based on the data of 2002 that calculates the VSF as a function of the scattering and backscattering. This model gives an estimate of the VSF with the specified scattering and backscattering values like the FF parameterization. The model can also take additional absorption data into account. We developed the same parameterization for all VSF wavelengths as far as shapes of VSF measured for different wavelengths are similar and the difference is significantly less than standard deviation (see Table 1).

To construct the optimal estimate of the VSF β as a function of scattering b and backscattering b_b, we have to note that b and b_b are linear functions of β. Indeed, the operations of numerical integration of Eq. (3) and Eq. (4) are the weighted summation of the components of VSF vector $\boldsymbol{\beta}$, which has a dimension M :

#120150 - $15.00 USD Received 30 Nov 2009; revised 6 Jan 2010; accepted 12 Jan 2010; published 22 Feb 2010

$$b = \sum_{i=0}^{M} \alpha_i^b \beta_i,$$
$$b_b = \sum_{i=M_{90}}^{M} \alpha_i^{bb} \beta_i, \tag{14}$$

where M_{90} is the index corresponding to angle value closest to $\pi/2$. The weights α_i^b and α_i^{bb} are the rows of matrix $\mathbf{A}$ in the Eq. (8), they are defined by the integration scheme, $\mathbf{b} = (b_b, b)^T$. We employed the trapezoidal numerical integration scheme to calculate α_i^b and α_i^{bb} [21].

Equation (14) defines *N-2* dimensional subspace in the *N*-dimensional space of the components of VSF. The best estimate of the VSF in that subspace obtained on the basis of the statistical data is defined by expressions in Eq. (6) and Eq. (9):

$$\hat{\boldsymbol{\beta}}_{bb,b} = \boldsymbol{\beta}^0 + \hat{\mathbf{R}}_{\mathbf{b}}^{\mathbf{A}} \cdot (\mathbf{b} - \mathbf{b}^0), \tag{15}$$

where $\boldsymbol{\beta}^0$ presented in the Table 1, $\mathbf{b} = (b_b, b)^T$ is a measured vector containing backscattering and scattering. The averaged components of $\mathbf{b}^0 = E(\mathbf{b}) = (b_b{}^0, b^0)^T$ are presented in the Table 2. The values of the elements of matrix $\hat{\mathbf{R}}_{\mathbf{b}}^{\mathbf{A}}$ calculated on the basis of Eq. (9) can be found in the Appendix.

To control the statistical quality of the proposed parameterization, we studied the ratio of the residual variance and the variance:

$$\chi = \frac{\mathrm{tr}(\mathbf{S}_{\delta\beta\,\delta\beta})}{\mathrm{tr}(\mathbf{S}_{\beta\beta})}, \tag{16}$$

where $\mathbf{S}_{\beta\beta}$ and $\mathbf{S}_{\delta\beta\,\delta\beta}$ are the covariance matrices of measured VSFs and errors of our model, Eq. (15) and $\boldsymbol{\delta\beta}_{bb,b} = \boldsymbol{\beta} - \hat{\boldsymbol{\beta}}_{bb,b}$. This ratio for our parameterization and the 95% confidence interval estimated by bootstrapping technique are:

$$\chi_{bb,b} = 0.57, \tag{17}$$

$$\mathrm{CI}(\chi_{bb,b}) = (0.36; 0.75). \tag{18}$$

The confidence interval shows that the estimate $\hat{\mathbf{R}}_{\mathbf{b}}^{\mathbf{A}}$ is statistically stable.

The proposed parameterization requires the values of the backscattering coefficients and the scattering coefficients which necessarily depend on the wavelength. Thus, the spectral variation of the VSF is obviously taken into account within the methodology. The final parameterization could be used at any wavelengths. The averaging that is used in the proposed method mostly concerns the average carried out over the number of VSF data (i.e. number of samples) and not necessarily over the spectral range of the VSF. It should be highlighted that the main goal of the parameterization developed in this study is to use in situ measurements to account for the major physical processes responsible for the variations of the VSF in natural waters (e.g., size distribution of particles, refractive index). The variability in the VSF (see Table 1 and Fig. 2), scattering and backscattering (see Table 2 and [17]) due to changes in the optical properties of the particles (e.g., nature and composition of the particles) at a given wavelength is much higher than the spectral variability in the VSF, scattering and backscattering Therefore, even if the spectral variation of the VSF would not be correctly

#120150 - $15.00 USD Received 30 Nov 2009; revised 6 Jan 2010; accepted 12 Jan 2010; published 22 Feb 2010

taken into account in our methodology (which is not the case), the impact of this spectral variation will be minor in the parameterization of the VSF since the latter will be much more influenced by the size and composition of the particles.

The approach described in this study can be easily applied for another data set and generalized for other types of scattering measurements. If some measurements are available, which have explicit linear dependence on VSF – Eq. (8), the matrix $\hat{\mathbf{R}}_{\mathbf{b}}^{\mathbf{A}}$ in Eq. (9) can be easily computed by our data. An example is the data of the ECO-VSF instrument designed by Wet Labs Inc., which performs the measurements of the scattered radiation at three fixed angles at low angular resolution. Similar to scattering and backscattering, these measurements can be expressed explicitly as integrals of the VSF which should be retrieved.

The more precise VSF model can be constructed with the use of some supplementary data in addition to scattering and backscattering, which has no explicit linear dependence on VSF. In that case we cannot calculate the rows of matrix $\mathbf{A}$ like in Eq. (14); thus, we should use Eq. (7) rather than Eq. (9) to calculate the regression matrix.

In some numerical models of radiative transfer in water such as Hydrolight [25], the VSF is calculated as a function of Chlorophyll concentration - $\beta(C_{chl})$ [25, 26]. As far as we have in situ chlorophyll concentration data corresponding to VSF measurements we tried to improve the VSF simulation using correlations with chlorophyll. It appears, however, that the scattering process is defined in general by non-algal particles and correlations between β and C_{chl} are weak (less than 0.4).

During the experiment at the platform the particulate spectral absorption was also regularly measured. The absorption and scattering processes are both defined by the properties of suspended matter. Thus VSF, scattering, backscattering and absorption are interconnected quantities. On the other hand, there is no exact linear dependence between scattering and absorption coefficients. Thus, one can expect significant partial correlations between VSF and spectral absorption given the scattering and backscattering. This fact is confirmed by previous studies [17, 18].

Finally we selected scattering, backscattering and spectral particular absorption at the wavelengths of the AC-9 instrument as the arguments for the VSF model. This is quite natural, because it is easier to measure scattering, backscattering and spectral absorption than VSF.

The same predictors were used in recent parameterization [7] of Freda and Piskozub. This work is based on fitting of FF phase functions to the VSFs measured in the Southern Baltic. Each FF phase function can be defined by two parameters: by Junge slope μ and refractive index n. Many phase functions were calculated for a wide range of μ and n values. After that only the (μ, n) pairs that fitted VSF were selected. A linear dependency was found between the absorption coefficient a measured by the mean of AC-9 values and $(n-1)/(\mu-3)$ factor. Finally the (μ, n) pair is retrieved by this linear fitting and by the backscatter fraction $B_p = b_b / b$. That defines the parameterization output - final FF phase function.

It appears that FF phase function generated by (μ, n) pairs fits well our VSF data. Nevertheless the hypothesis of linear dependence of absorption data and $(n-1)/(\mu-3)$ factor can be rejected (see Fig. 6). The 95% confidence interval comprises a horizontal line, thus linear dependence cannot be established. We also fail to find other combinations of spectral absorptions which provide linear dependence. Thus, the method proposed in [7] cannot be applied to our data.

#120150 - $15.00 USD Received 30 Nov 2009; revised 6 Jan 2010; accepted 12 Jan 2010; published 22 Feb 2010

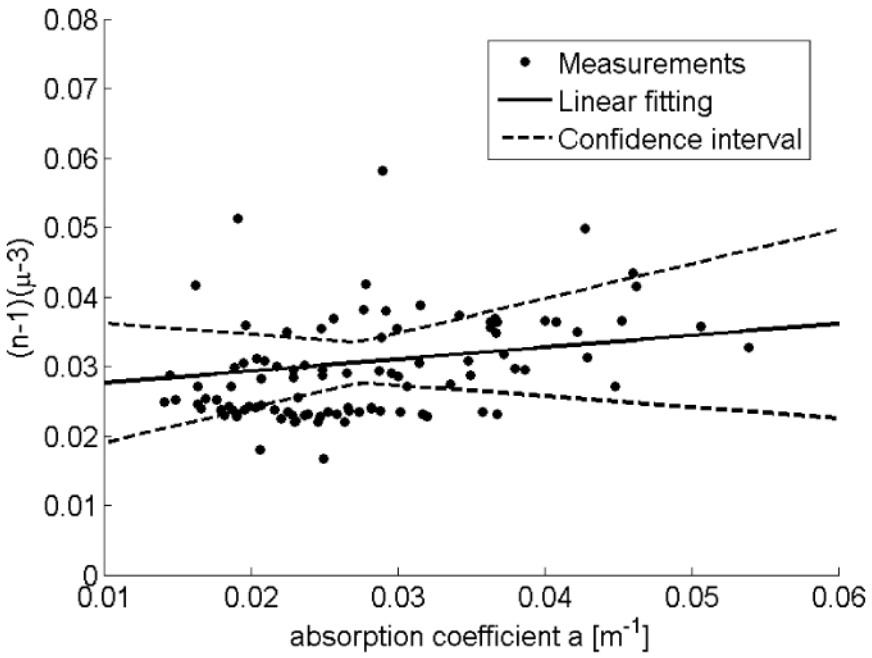

Fig. 6. The factor (n-1)/(μ-3) plotted with absorption coefficients for a wavelength 555 nm and the attempt of linear fitting. The horizontal line lies within 95% confidence interval and a linear dependence cannot be established.

In our parameterization we used the linear estimation technique to account for the absorption data. The idea is to obtain more accurate VSF estimate than $\hat{\boldsymbol{\beta}}_{bb,b}$ in Eq. (15) by the additional absorption data,

$$\hat{\boldsymbol{\beta}}_{bb,b,a} = \hat{\boldsymbol{\beta}}_{bb,b} + \delta\hat{\boldsymbol{\beta}}_{bb,b,a}, \tag{19}$$

provided that the specific backscattering and scattering values are conserved:

$$\mathbf{A}\hat{\boldsymbol{\beta}}_{bb,b,a} = \begin{pmatrix} b_b \\ b \end{pmatrix}. \tag{20}$$

We use again the regression estimation like in Eq. (6), Eq. (7):

$$\delta\hat{\boldsymbol{\beta}}_{bb,b,\mathbf{a}} = \hat{\mathbf{R}}_{\mathbf{a}} \cdot \left(\mathbf{a} - \mathbf{a}^0\right), \tag{21}$$

$$\hat{\mathbf{R}}_{\mathbf{a}} = \mathbf{S}_{\delta\boldsymbol{\beta}\mathbf{a}}\mathbf{S}_{\mathbf{a}}^{-1}, \tag{22}$$

where $\delta\boldsymbol{\beta}$ is the error of parameterization defined in Eq. (15),

$$\delta\boldsymbol{\beta} = \boldsymbol{\beta} - \hat{\boldsymbol{\beta}}_{bb,b}, \tag{23}$$

$\mathbf{a}^0 = E(\mathbf{a})$, $\mathbf{S}_{\delta\boldsymbol{\beta}\mathbf{a}}$ and $\mathbf{S}_{\mathbf{a}}$ are the covariance matrixes.

The final expression for the parameterization which account for backscattering, scattering and absorption data is:

$$\hat{\boldsymbol{\beta}}_{bb,b,\mathbf{a}} = \boldsymbol{\beta}^0 + \hat{\mathbf{R}}_{\mathbf{b}}^{\mathbf{A}} \cdot \left(\mathbf{b} - \mathbf{b}^0\right) + \hat{\mathbf{R}}_{\mathbf{a}} \cdot \left(\mathbf{a} - \mathbf{a}^0\right), \tag{24}$$

#120150 - $15.00 USD Received 30 Nov 2009; revised 6 Jan 2010; accepted 12 Jan 2010; published 22 Feb 2010

where mean values of VSF $\boldsymbol{\beta}^0$, backscatter and scatter $\mathbf{b}^0 = \left(b_b^0, b^0\right)^T$, particulate spectral absorption $\mathbf{a}^0$ are presented in Table 1, Table 2, Table 3 respectively. The matrixes $\hat{\mathbf{R}}_{\mathbf{b}}^{\mathbf{A}}$ and $\hat{\mathbf{R}}_{\mathbf{a}}$ can be found in Appendix.

Multiplying the Eq. (23) by matrix $\mathbf{A}$ we can find by Eq. (8) and Eq. (11) that $\delta\boldsymbol{\beta}$ is orthogonal to the rows of $\mathbf{A}$.

$$\mathbf{A} \cdot \delta\boldsymbol{\beta} = 0. \tag{25}$$

As far as the regression estimate $\delta\hat{\boldsymbol{\beta}}_{bb,b,\mathbf{a}}$ in Eq. (21) belongs to the same subspace as the initial $\delta\boldsymbol{\beta}$, $\delta\hat{\boldsymbol{\beta}}_{bb,b,\mathbf{a}}$ and is also orthogonal to the rows of $\mathbf{A}$:

$$\mathbf{A} \cdot \delta\hat{\boldsymbol{\beta}}_{bb,b,\mathbf{a}} = 0. \tag{26}$$

Multiplying Eq. (24) by $\mathbf{A}$ subject to Eq. (21) and Eq. (10) we find that the Eq. (20) is satisfied. Hence our parameterization conserves scattering and backscattering values.

We calculated again the value χ (16), $\delta\boldsymbol{\beta}_{bb,b,\mathbf{a}} = \boldsymbol{\beta} - \hat{\boldsymbol{\beta}}_{bb,b,\mathbf{a}}$ and the 95% confidence interval:

$$\chi_{bb,b,\mathbf{a}} = 0.51, \tag{27}$$

$$\mathrm{CI}\left(\chi_{bb,b,\mathbf{a}}\right) = \left(0.32; 0.68\right). \tag{28}$$

The values calculated for the parameterization presented by Eq. (24) are less than for the parameterization without absorption defined in Eq. (15). It proves that employing absorption measurements accounts for more of the VSF variability..

We applied the cross-validation method to avoid the overfitting problem. The point estimates of the error variance normalized by VSF variance obtained from the cross-validation and calculated by the standard method from the total ensemble are shown in Fig. 7. The confidence intervals are also constructed at the 0.95 confidence level for the cross-validation error estimate. We can see that the values of normalized error variance calculated by total ensemble lies within the cross-validation confidence interval. It shows that the difference between the point estimates is not significant. Thus, we can rely that the standard *a priori* estimate of the parameterization error is not underestimated due to the overfiting problem.

#120150 - $15.00 USD Received 30 Nov 2009; revised 6 Jan 2010; accepted 12 Jan 2010; published 22 Feb 2010

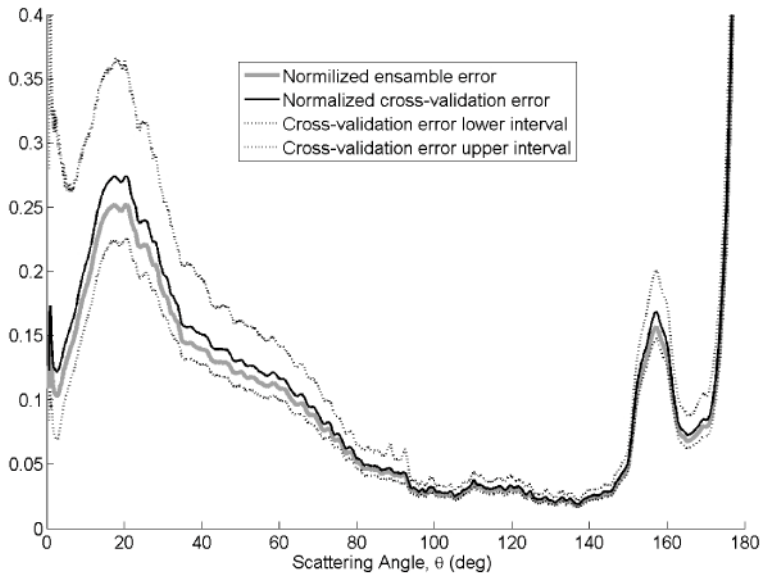

Fig. 7. Confidence intervals and point estimates for normalized error variances obtained by cross-validation method and by the standard method from the total calibration ensemble.

The error of the parameterization strongly depends on the scattering angle. The most significant errors are concentrated at extreme angles, because the extrapolation [20] is used for this angular range. The error growth at 155° corresponds to a small VSF hump, the particularity of our data set (see Fig. 3 and Fig. 4).

5. Elements of linear estimation matrix

As far as the numerical values of VSF, backscattering, scattering and absorption ranges from 10^{4} to 10^{-3}, it is not convenient to directly consider the elements of $\hat{\mathbf{R}}_{\mathbf{b}}^{\mathbf{A}}$ and $\hat{\mathbf{R}}_{\mathbf{a}}$. Instead, we analyzed the elements of modified matrixes $\tilde{\mathbf{R}}_{\mathbf{b}}^{\mathbf{A}}$ and $\tilde{\mathbf{R}}_{\mathbf{a}}$, which relate normalised VSF, VSF error Eq. (23) and normalised backscattering, scattering and absorption. After the transforms $\tilde{\boldsymbol{\beta}} = \boldsymbol{\Delta}_{\boldsymbol{\beta}}^{-1}\boldsymbol{\beta}$ and $\tilde{\mathbf{b}} = \boldsymbol{\Delta}_{\mathbf{b}}^{-1}\mathbf{b}$, we can find that these matrixes are represented as follows:

$$\tilde{\mathbf{R}}_{\mathbf{b}}^{\mathbf{A}} = \boldsymbol{\Delta}_{\boldsymbol{\beta}}^{-1}\hat{\mathbf{R}}_{\mathbf{b}}^{\mathbf{A}}\boldsymbol{\Delta}_{\mathbf{b}},\ \boldsymbol{\Delta}_{\boldsymbol{\beta}} = \mathrm{diag}\left(\sigma\left(\boldsymbol{\beta}\right)\right),\ \boldsymbol{\Delta}_{\mathbf{b}} = \mathrm{diag}\left(\sigma\left(\mathbf{b}\right)\right), \tag{29}$$

$$\tilde{\mathbf{R}}_{\mathbf{a}} = \boldsymbol{\Delta}_{\delta\boldsymbol{\beta}}^{-1}\hat{\mathbf{R}}_{\mathbf{a}}\boldsymbol{\Delta}_{\mathbf{a}},\ \boldsymbol{\Delta}_{\delta\boldsymbol{\beta}} = \mathrm{diag}\left(\sigma\left(\boldsymbol{\beta} - \hat{\boldsymbol{\beta}}_{bb,b}\right)\right),\ \boldsymbol{\Delta}_{\mathbf{a}} = \mathrm{diag}\left(\sigma\left(\mathbf{a}\right)\right), \tag{30}$$

where $\mathrm{diag}\left(\sigma\right)$ denotes diagonal matrix with elements of σ on the diagonal, σ is a vector of standard deviations.

The elements of matrix $\tilde{\mathbf{R}}_{\mathbf{b}}^{\mathbf{A}}$ presented in Fig. 8. Large absolute values correspond to significant contribution to VSF variability. We can see that the backscattering provides information over the entire angular range with the exception of small angles (< 30°). Meanwhile, the scattering contributes at the angles smaller than 10°. This can be explained by huge VSF values at small angles, so the majority of light is scattered to the small angles. We note also that backscattering and scattering contribution to VSF variability is less at angular ranges (10°, 30°) and (150°, 180°) . That can be explained by $\sin\left(\theta\right)$ term in Eq. (3) and Eq. (4).

#120150 - $15.00 USD Received 30 Nov 2009; revised 6 Jan 2010; accepted 12 Jan 2010; published 22 Feb 2010

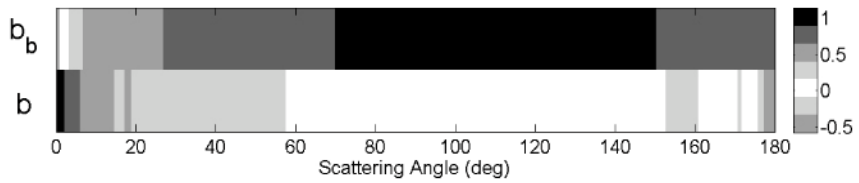

Fig. 8. Elements of transposed matrix $\tilde{\mathbf{R}}_{\mathbf{b}}^{\mathbf{A}}$.

The elements of matrix $\tilde{\mathbf{R}}_{\mathbf{a}}$, presented in Fig. 9, shows that a portion of information on the VSF variability at small angles (5°, 50°) and high angles (165°-180°) can be retrieved from absorption data. That's why the parameterization in Eq. (24), which accounts for absorption data is in general more exact at extreme angles than the other technique in Eq. (15), the reduction of error reaches up to 10% of the total VSF value at high angles. The channels from 440 nm (maximum of chlorophyll absorption) to 555 nm (minimum of chlorophyll absorption) are the most informative.

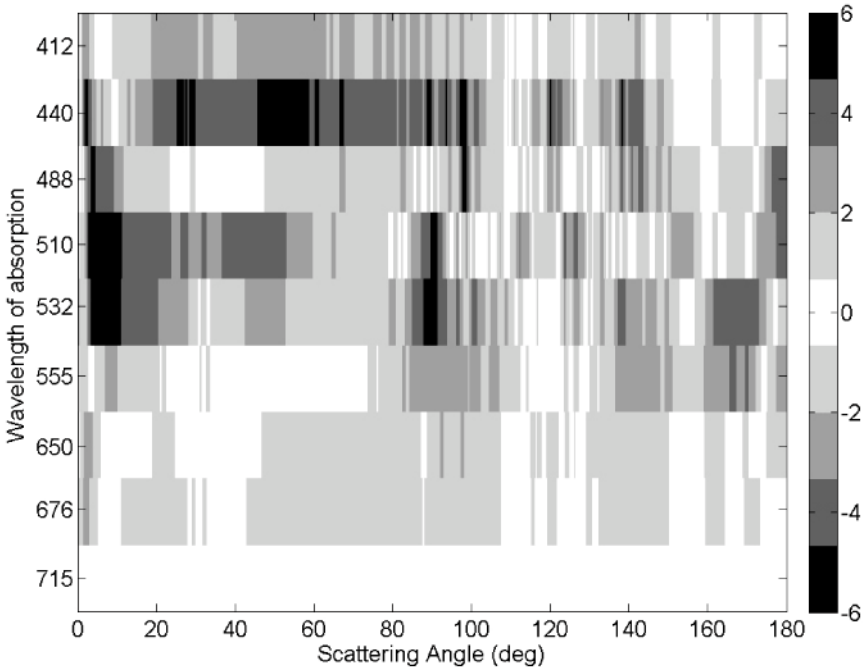

Fig. 9. Elements of transposed matrix $\tilde{\mathbf{R}}_{\mathbf{a}}$.

We note again, that our parameterization conserves scattering and backscattering in a similar manner to the FF approach. It means that scattering and backscattering calculated by the simulated VSF profile are equal to input scattering and backscattering.

6. Results and discussion

We used two quantities for the estimation of the accuracy of the following VSF modeling methods: the first is our parameterization, then scaling of the mean VSF measured in 2002, scaling of Petzold measurements [4] and FF fitting [2].

The expression for the relative error $\delta(\theta)$, which is a relative root mean square error at angle θ is the following:

#120150 - $15.00 USD Received 30 Nov 2009; revised 6 Jan 2010; accepted 12 Jan 2010; published 22 Feb 2010

$$\delta(\theta)=\sqrt{\frac{1}{N_m}\sum_{i=1}^{N_m}\left(\frac{\beta^i(\theta)-\hat{\beta}^i(\theta)}{\beta^i(\theta)}\right)^2}\cdot\sin(\theta), \tag{31}$$

where N_m is the number of VSF measurements $\beta^i(\theta)$ and $\hat{\beta}^i(\theta)$ are respectfully a measurement and a simulation. The relative error $\delta(\theta)$ presented in Fig. 10 for the full range of angles. We introduce here the weight $\sin(\theta)$ similar to the definitions of scattering Eq. (3) and backscattering Eq. (4). Following the results of Freda and Piskozub [7] this is necessary for reducing the sensitivity of $\delta(\theta)$ to errors at extreme angles, where the measurements are less stable.

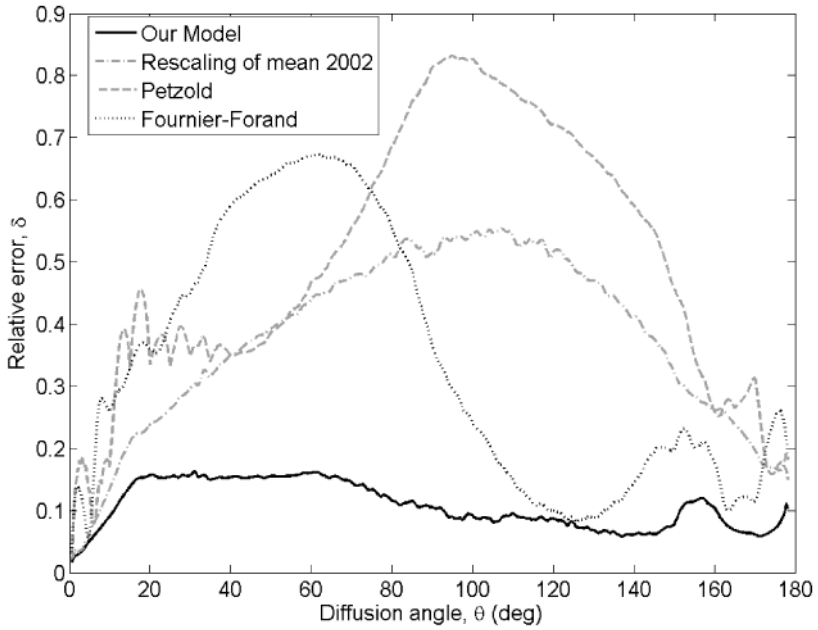

Fig. 10. The relative error *δ(θ)* of the considered VSF parameterizations calculated by the data of 2002.

The total relative error δ_{tot}, that characterises the total performance of the parameterization is the root mean square value of $\delta(\theta_j)$:

$$\delta_{tot}=\sqrt{\frac{1}{M}\sum_{j=1}^{M}\delta(\theta_j)^2}, \tag{32}$$

where $M\approx 600$ is the number of angles resolved by the VSM, and is equal to the dimension of non-extrapolated vectors $\boldsymbol{\beta}_v$ and $\boldsymbol{\beta}_v^0$, $\theta_j\in[0.7°,178°]$.

The values of total relative error δ_{tot} calculated for the considered models on the basis of the data of 2002 are presented in the second row of Table 4. Our model gives the best result at full range of angles. The rescaling of mean value also gives a good result because the shapes of measurements at 2002 are similar. The FF parameterization that was designed to fit well the backscattering is, as expected, more precise at $\theta>90°$. The retrieval based on recalibration of Petzold phase function is the less exact.

#120150 - $15.00 USD Received 30 Nov 2009; revised 6 Jan 2010; accepted 12 Jan 2010; published 22 Feb 2010

Table 4. The total relative error δ_{tot} in percent of the retrieval by different techniques.*

Year	Number of samples	**Our model**	Rescaling of mean VSF 2002	Rescaling of Petzold VSF (coastal ocean)	Fournier-Forand backscattering to scattering fitting
2002	404	**12%**	40%	54%	39%
2003	140	**11%**	53%	24%	18%
2004	54	**9%**	36%	23%	25%

*The proposed model (third column marked by boldface) and rescaling technique (fourth column) are based on data of 2002. The data measured in 2002, 2003 and 2004 were used for the validation.

In order to estimate the reliability of our parameterization, we carried out an independent validation. We employed the VSF data measured during the campaign of 2003 and 2004. We obtained 140 samples for the data of 2003 and 54 samples for 2004 after the selection of the samples for which we had the absorption data and the application of the filtration procedure Eq. (12). The instrument calibration was slightly changed and there is no perfect coincidence of the forms of VSF especially at high angles. In addition, the measurements of 2004 are less stable and the VSFs have some oscillations.

The proposed technique was compared again with rescaling, Petzold, and FF fitting. We have calculated again the values of total relative error δ_{tot} Eq. (32) for the data of 2003 and 2004. These results are presented in the third and fourth rows of Table 4. In general the accuracy of all the techniques remained at the same level or increased. The possible explanation is a diversity of the meteorological conditions and the complexity of water types in the data of 2002 in comparison with the data of 2003 and 2004. So the parameterisations fit, in general, better the data of 2003 and 2004. The typical examples of the retrieved and the original VSF measured in 2003 are presented in Fig. 11.

The angular dependence of the relative error $\delta(\theta)$ for 2003 and 2004 data is shown in Fig. 12 and Fig. 13 respectively. The curves are similar to the relative error of 2002 (Fig. 10). The obtained results also attest that the proposed parameterization is suitable to reproduce the VSF of a variety of water types similar to the Black Sea coastal area.

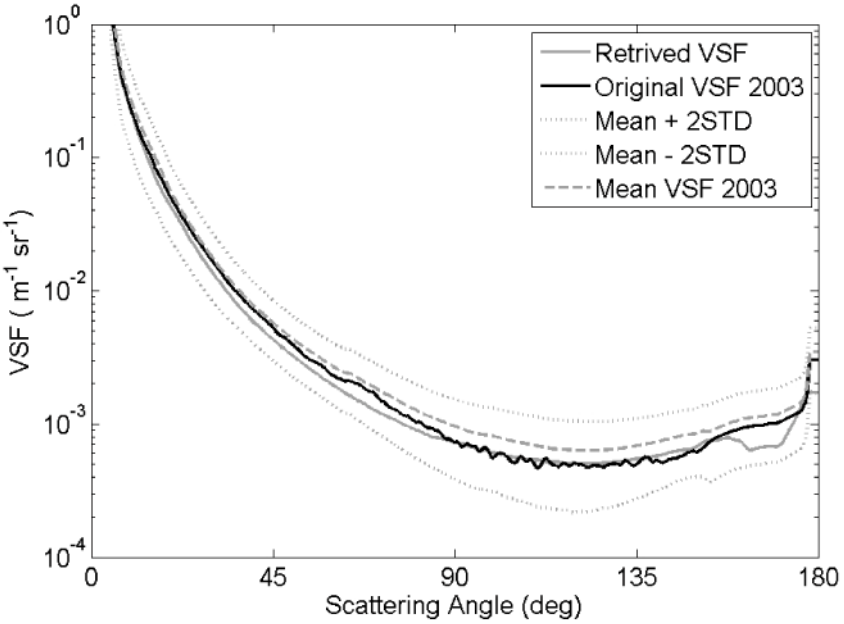

Fig. 11. Example of retrieval of VSF measured in 2003 at 555 nm. The mean of VSF 2003 and doubled root mean squared deviation is also presented.

#120150 - $15.00 USD Received 30 Nov 2009; revised 6 Jan 2010; accepted 12 Jan 2010; published 22 Feb 2010

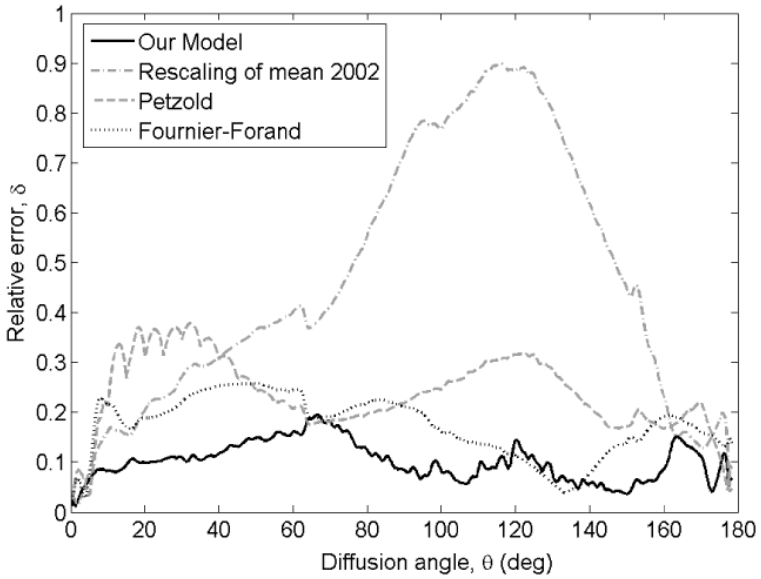

Fig. 12. The relative error $\delta(\theta)$ of the VSF parameterizations calculated by the data of 2003.

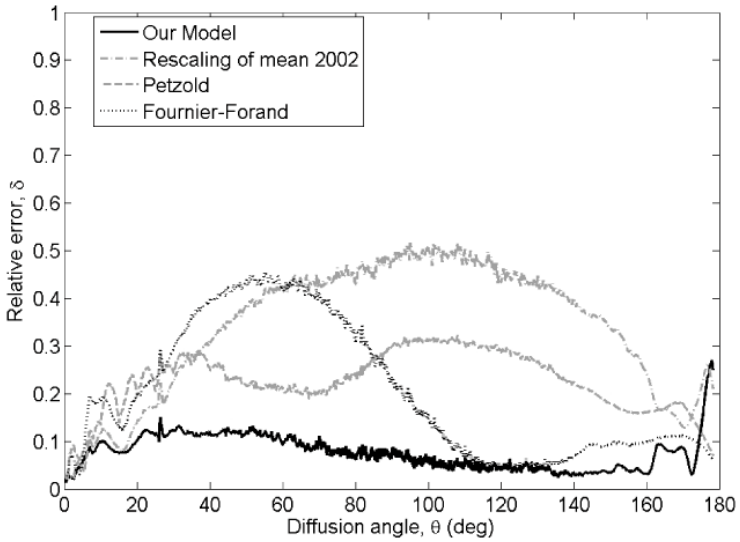

Fig. 13. The relative error $\delta(\theta)$ of the VSF parameterizations calculated by the data of 2004.

Conclusions and perspectives

We have proposed a parameterization based on real VSF measurements in the Black Sea coastal area. If the measurements of scattering, backscattering and (optionally) absorption are known, the VSF can be retrieved with relative error value less than 15%. The proposed parameterization is constructed of a representative measurement data set and has the important property of conserving the scattering and backscattering values. The comparisons showed that for the waters similar to Black sea coastal waters our technique is more powerful than common Petzold and Fournier-Forand fitting. Our model can be used for Rrs simulations by different radiative transfer codes such as, for instance, Hydrolight.

#120150 - $15.00 USD Received 30 Nov 2009; revised 6 Jan 2010; accepted 12 Jan 2010; published 22 Feb 2010

Acknowledgments

The work was funded by National Center of Space Research of France (CNES) and SESAM project. We are grateful to the anonymous reviewers for their relevant comments and suggestions. We would like to thank also M.E.-G. Lee, E.B. Shybanov, O.V. Martynov, T.Y. Churilova, G.K. Korotaev and all the team that collected the data in the Black Sea.

Appendix.

Table 5. Elements of Matrix R_b^{A*}.

−6.38E+06	1.74E+05
−1.23E+05	3.81E+03
−1.71E+04	6.72E+02
−4.03E+03	2.31E+02
−3.64E+02	8.66E+01
−9.40E+01	5.80E+01
9.89E+01	3.42E+01
1.37E+02	1.28E+01
7.96E+01	3.02E+00
2.24E+01	3.88E-01
1.05E+01	1.31E-01
4.96E+00	5.95E-02
2.90E+00	2.85E-02
2.01E+00	1.57E-02
1.01E+00	5.71E-03
6.05E-01	2.48E-03
4.05E-01	1.15E-03
2.96E-01	5.46E-04
2.34E-01	1.58E-04
1.94E-01	1.87E-05
1.73E-01	−1.21E-04
1.60E-01	−1.59E-04
1.54E-01	−1.60E-04
1.52E-01	−3.30E-05
1.54E-01	7.34E-05
1.46E-01	3.48E-04
1.21E-01	4.60E-04
1.25E-01	4.96E-04
1.48E-01	4.24E-04
1.58E-01	5.12E-04
1.69E-01	5.47E-04
1.98E-01	1.53E-04
2.22E-01	−1.78E-04
2.59E-01	−7.95E-04
2.95E-01	−2.04E-03
3.09E-01	−2.66E-03
3.24E-01	−3.37E-03
3.47E-01	−4.36E-03
3.47E-01	−4.38E-03
3.47E-01	−4.38E-03

*The rows correspond to angles presented in Table 1. The columns correspond to scattering and backscattering.

#120150 - $15.00 USD Received 30 Nov 2009; revised 6 Jan 2010; accepted 12 Jan 2010; published 22 Feb 2010

Table 6. Elements of Matrix R_a ***.**

d3.88E+5	−1.16E+6	3.26E+6	−7.68E+6	6.68E+6	2.93E+5	−7.53E+6	2.63E+6	5.88E+6
5.57E+3	−1.26E+4	2.36E+4	−7.55E+4	7.93E+4	4.55E+3	−9.49E+4	3.58E+4	8.65E+4
3.15E+2	−6.89E+2	7.15E+2	−3.89E+3	6.12E+3	−7.98E+2	−6.42E+3	2.43E+3	7.09E+3
−1.87E+2	2.83E+2	−4.14E+1	1.90E+2	4.57E+2	−9.39E+2	8.48E+2	−5.30E+2	−4.28E+2
−1.17E+2	1.31E+2	2.65E+2	3.27E+2	−4.05E+2	−6.77E+2	1.22E+3	−5.64E+2	−5.76E+2
−2.01E+2	3.78E+2	−1.16E+2	2.52E+2	−2.35E+2	−4.32E+2	1.62E+3	−7.82E+2	−1.88E+3
−1.13E+2	2.39E+2	−1.88E+2	2.62E+2	−2.06E+2	−1.87E+2	1.09E+3	−4.75E+2	−1.39E+3
−2.79E+1	7.36E+1	−1.30E+2	2.26E+2	−1.86E+2	−2.57E+1	3.71E+2	−1.37E+2	−4.53E+2
−1.47E+0	1.02E+1	−3.92E+1	8.07E+1	−8.39E+1	2.27E+1	4.73E+1	−1.34E+1	−5.11E+1
1.05E+0	−6.98E-1	−5.47E+0	1.30E+1	−1.63E+1	8.47E+0	−3.16E+0	2.89E+0	1.50E+1
8.38E-1	−1.29E+0	−1.54E+0	5.37E+0	−5.83E+0	2.33E+0	−2.28E+0	2.14E+0	8.39E+0
5.17E-1	−9.51E-1	−3.31E-1	2.47E+0	−2.57E+0	8.75E-1	−1.75E+0	1.19E+0	3.78E+0
2.82E-1	−6.18E-1	1.04E-1	8.52E-1	−8.03E-1	2.14E-1	−7.37E-1	5.45E-1	1.74E+0
1.47E-1	−3.71E-1	9.05E-2	4.29E-1	−1.73E-1	−9.99E-2	−2.34E-1	2.02E-1	4.71E-1
5.03E-2	−1.26E-1	9.52E-3	2.12E-1	−9.28E-2	−4.63E-2	−1.28E-1	7.19E-2	3.14E-1
3.58E-2	−9.32E-2	3.22E-2	1.27E-1	−8.81E-2	−3.00E-4	−1.17E-1	6.60E-2	1.89E-1
1.80E-2	−4.62E-2	3.01E-2	2.90E-2	−1.68E-2	−5.44E-3	−1.01E-1	4.47E-2	1.64E-1
9.91E-3	−2.54E-2	1.94E-2	1.02E-2	−1.52E-2	1.08E-2	−5.12E-2	2.32E-2	3.53E-2
6.02E-3	−1.40E-2	1.31E-2	−4.64E-4	−1.52E-2	1.86E-2	−2.40E-2	1.16E-2	2.07E-3
4.34E-3	−1.14E-2	1.29E-3	3.06E-2	−4.00E-2	2.24E-2	−2.05E-2	1.12E-2	−1.02E-2
2.30E-3	−5.72E-3	7.67E-3	−2.28E-3	−1.19E-2	1.45E-2	−2.49E-2	9.48E-3	3.88E-2
3.91E-4	−2.93E-4	3.01E-3	−6.56E-3	−3.39E-3	8.34E-3	−7.89E-3	3.68E-3	3.54E-4
−1.94E-3	7.42E-3	−6.94E-3	−6.81E-3	5.79E-3	−1.91E-4	1.75E-2	−6.63E-3	−2.26E-2
−1.13E-3	1.84E-3	−1.63E-3	2.35E-3	3.35E-4	−4.14E-3	1.03E-2	−3.33E-3	−2.29E-3
−1.81E-3	4.81E-3	−4.33E-3	−3.15E-3	1.32E-2	−1.35E-2	1.87E-2	−7.22E-3	−9.79E-3
−1.51E-3	3.58E-3	−5.89E-3	3.12E-3	1.61E-2	−1.98E-2	1.23E-2	−6.04E-3	2.12E-3
−3.60E-4	−6.90E-4	−4.24E-3	1.50E-2	3.84E-3	−1.56E-2	6.34E-3	−2.47E-3	−6.10E-3
−8.90E-4	4.72E-4	1.74E-3	−4.78E-3	2.51E-2	−2.83E-2	2.09E-2	−9.23E-3	4.42E-3
−4.88E-4	−2.34E-4	−4.68E-3	1.65E-3	3.27E-2	−3.40E-2	7.51E-3	−4.32E-3	2.27E-2
−1.03E-3	1.56E-3	−7.69E-3	−7.01E-4	4.33E-2	−4.22E-2	1.70E-2	−8.85E-3	1.09E-2
−2.70E-3	2.71E-3	2.35E-4	−1.98E-2	5.44E-2	−3.56E-2	1.74E-2	−1.49E-2	−4.13E-2
−3.34E-3	−2.84E-3	2.30E-2	−5.06E-2	5.65E-2	−4.01E-3	−2.79E-2	−9.73E-3	−1.27E-1
−2.61E-3	−1.00E-2	4.19E-2	−7.05E-2	5.50E-2	1.88E-2	−6.35E-2	−3.45E-3	−1.73E-1
−2.11E-3	−2.31E-2	8.03E-2	−1.04E-1	4.72E-2	5.70E-2	−1.37E-1	1.23E-2	−2.36E-1
−2.44E-3	−3.42E-2	1.24E-1	−1.43E-1	2.19E-2	1.14E-1	−2.16E-1	3.04E-2	−3.06E-1
−2.19E-3	−3.83E-2	1.41E-1	−1.57E-1	6.17E-3	1.40E-1	−2.49E-1	3.97E-2	−3.23E-1
−1.31E-3	−4.33E-2	1.59E-1	−1.74E-1	−1.32E-2	1.70E-1	−2.86E-1	5.12E-2	−3.34E-1
8.97E-4	−5.11E-2	1.86E-1	−1.99E-1	−4.38E-2	2.16E-1	−3.36E-1	6.77E-2	−3.37E-1
1.10E-3	−5.15E-2	1.87E-1	−2.00E-1	−4.44E-2	2.17E-1	−3.36E-1	6.80E-2	−3.37E-1
1.10E-3	−5.15E-2	1.87E-1	−2.00E-1	−4.44E-2	2.17E-1	−3.36E-1	6.80E-2	−3.37E-1

*The rows correspond to angles presented in Table 1. The columns correspond to channels of Wetlabs AC-9 instrument presented in Table 3.

#120150 - $15.00 USD Received 30 Nov 2009; revised 6 Jan 2010; accepted 12 Jan 2010; published 22 Feb 2010